Theoretical and experimental analysis of excessively tilted fiber gratings

Zhijun Yan,[1,2] Hushan Wang,[1] Changle Wang,[2] Zhongyuan Sun,[2] Guolu Yin,[2] Kaiming Zhou,[1,2] Yishan Wang,[1,*] Wei Zhao,[1] and Lin Zhang,[2,3]

[1]State Key Laboratory of Transient Optics and Photonics, Xi'an Institute of Optics and Precision Mechanics, Chinese Academy of Sciences, Xi'an 710119, China
[2]Institute of Photonic and Technologies, Aston University, Birmingham B4 7ET, UK
[3]l.zhang@aston.ac.uk
[*]yshwang@opt.ac.cn

Abstract: We have theoretically and experimentally investigated the dual-peak feature of tilted fiber gratings with excessively tilted structure (named as Ex-TFGs). We have explained the dual-peak feature by solving eigenvalue equations for TM_{0m} and TE_{0m} of a circular waveguide, in which the TE (transverse electric) and TM (transverse magnetic) core modes are coupled into TE and TM cladding modes, respectively. Meanwhile, in the experiment, we have verified that one of the dual peaks at the shorter wavelength is due to the TM mode coupling whereas the other one at the longer wavelength arises from TE mode coupling when a linearly polarized light launched into the Ex-TFG. We have also investigated the peak separation of TE and TM cladding mode for different surrounding medium refractive indexes (SRI), revealed that the dual peaks separation is decreasing as increasing of SRI, which agrees very well with the theoretical analysis results.

©2016 Optical Society of America

OCIS codes: (060.0060) Fiber optics and optical communications; (060.2370) Fiber optics sensors; (230.5440) Polarization-selective devices.

References and links

1. K. O. Hill, Y. Fujii, D. C. Johnson, and B. S. Kawasaki, "Photonsensitivity in optical fibre waveguides: Application to reflection filter fabrication," Appl. Phys. Lett. **32**(10), 647–649 (1978).
2. G. Meltz, W. W. Morey, and W. H. Glenn, "In-fibre Bragg grating tap," *Optical Fibre Communications Conference*, 1990 OSA Technical Digest Series (Optical Society of America, 1990), paper TuG1.
3. J. Albert, L. Y. Shao, and C. Caucheteur, "Tilted fiber Bragg gratings sensors," Laser Photonics Rev. **7**(1), 83–108 (2013).
4. Y. Miao, B. Liu, H. Zhang, Y. Li, H. Zhou, H. Sun, W. Zhang, and Q. Zhao, "Relative humidity sensor based on tilted fiber Bragg grating with polyvinyl alcohol coating," IEEE Photonics Technol. Lett. **21**(7), 441–443 (2009).
5. T. Guo, L. Shao, H.-Y. Tam, P. A. Krug, and J. Albert, "Tilted fiber grating accelerometer incorporating an abrupt biconical taper for cladding to core recoupling," Opt. Express **17**(23), 20651–20660 (2009).
6. B. Gu, W. Qi, Y. Zhou, Z. Wu, P. P. Shum, and F. Luan, "Reflective liquid level sensor based on modes conversion in thin-core fiber incorporating tilted fiber Bragg grating," Opt. Express **22**(10), 11834–11839 (2014).
7. K. Zhou, G. Simpson, X. Chen, L. Zhang, and I. Bennion, "High extinction ratio in-fiber polarizers based on 45 ° tilted fiber Bragg gratings," Opt. Lett. **30**(11), 1285–1287 (2005).
8. Z. Yan, K. Zhou, and L. Zhang, "In-fiber linear polarizer based on UV-inscribed 45° tilted grating in polarization maintaining fiber," Opt. Lett. **37**(18), 3819–3821 (2012).
9. I. Peupelmann, E. Krause, A. Bandemer, and C. Schaffer, "Fibre-polarimeter based on grating taps," Electron. Lett. **38**(21), 1248–1250 (2002).
10. K. Zhou, X. Cheng, Z. Yan, A. Adedotun, and L. Zhang, "Optical spectrum analyzer using a 45° tilted fiber grating," in *Advanced Photonics Congress,* OSA Technical Digest (online) (Optical Society of America, 2012), paper BW2E.7.
11. A. Adebayo, Z. Yan, K. Zhou, L. Zhang, H. Fu, and D. Robinson, "Power tapping function in near infra-red region based on 45° tilted fiber gratings," Opt. Photonics J. **3**(02), 158 (2013).
12. K. Zhou, L. Zhang, X. Chen, and I. Bennion, "Optic sensors of high refractive-index responsivity and low thermal cross sensitivity that use fiber Bragg gratings of >80 ° tilted structures," Opt. Lett. **31**(9), 1193–1195 (2006).

13. X. Chen, K. Zhou, L. Zhang, and I. Bennion, "In-fiber twist sensor based on a fiber Bragg grating with 81° tilted structure," IEEE Photonics Technol. Lett. **18**, 2596–2598 (2006).
14. R. Suo, X. Chen, K. Zhou, L. Zhang, and I. Bennion, "In-fibre directional transverse loading sensor based on excessively tilted fibre Bragg gratings," Meas. Sci. Technol. **20**(3), 034015 (2009).
15. K. Zhou, L. Zhang, X. Chen, and I. Bennion, "Optic sensors of high refractive-index responsivity and low thermal cross sensitivity that use fiber Bragg gratings of >80 ° tilted structures," Opt. Lett. **31**(9), 1193–1195 (2006).
16. C. Mou, K. Zhou, Z. Yan, H. Fu, and L. Zhang, "Liquid level sensor based on an excessively tilted fibre grating," Opt. Commun. **305**, 271–275 (2013).
17. Z. Yan, C. Mou, Z. Sun, K. Zhou, H. Wang, Y. Wang, W. Zhao, and L. Zhang, "Hybrid tilted fiber grating based refractive index and liquid level sensing system," Opt. Commun. **351**, 144–148 (2015).
18. L.-Y. Shao, Y. Shevchenko, and J. Albert, "Intrinsic temperature sensitivity of tilted fiber Bragg grating based surface plasmon resonance sensors," Opt. Express **18**(11), 11464–11471 (2010).
19. J. Albert, L.-Y. Shao, A. Beliaev, and C. Caucheteur, "Polarization properties of tilted fiber Bragg gratings for novel sensing modalities," Proc. SPIE **8028**, 802802 (2011).
20. C. Caucheteur, Y. Shevchenko, L.-Y. Shao, M. Wuilpart, and J. Albert, "High resolution interrogation of tilted fiber grating SPR sensors from polarization properties measurement," Opt. Express **19**(2), 1656–1664 (2011).
21. Q. Li, F. Yan, P. Liu, W. Peng, G. Yin, and T. Feng, "Analysis of transmission characteristics of tilted long period fiber gratings with full vector complex coupled mode theory," Photonic Sensors **2**(2), 158–165 (2012).
22. G. Yin, S. Lou, Q. Li, and H. Zou, "Theory analysis of mode coupling in tilted long period fiber grating based on the full vector complex coupled mode theory," Opt. Laser Technol. **48**, 60–66 (2013).
23. C. Mou, Z. Yan, K. Zhou, and L. Zhang, "Optical fibre sensors based on UV inscribed excessively tilted fibre grating," *Optical Sensors - New developments and Practical Applications*, Dr Moh. Yasin, Ed. (InTech, 2014).
24. B. Luo, Z. Yan, Z. Sun, J. Li, and L. Zhang, "Novel glucose sensor based on enzyme-immobilized 81° tilted fiber grating," Opt. Express **22**(25), 30571–30578 (2014).
25. J. Adams, *An Introduction to Optical Waveguides* (Wiley, 1981).
26. T. Erdogan, "Cladding-mode resonances in short- and long- period fibre grating filters," J. Opt. Soc. Am. A **14**(8), 1760–1773 (1997).
27. T. Erdogan and V. Mizrahi, "Characterization of UV-induced birefringence in photosensitive Ge-doped silica optical fibers," J. Opt. Soc. Am. B **11**(10), 2100–2105 (1994).
28. K. Zhou, X. Chen, L. Zhang, and I. Bennion, "Low thermal sensitivity grating devices based on Ex-45° tilting structure capable of forward-propagating cladding modes coupling," J. Lightwave Technol. **24**(12), 5087–5094 (2006).
29. X. Shu, L. Zhang, and I. Bennion, "Sensitivity characteristics of long-period fiber gratings," J. Lightwave Technol. **20**(2), 255–266 (2002).
30. T. W. MacDougall, S. Pilevar, C. W. Haggans, and M. A. Jackson, "Generalized expression for the growth of long period gratings," IEEE Photonics Technol. Lett. **10**(10), 1449–1451 (1998).
31. S. J. Mihailov, R. B. Walker, P. Lu, H. Ding, X. Dai, C. Smelser, and L. Chen, "UV-Induced polarization-dependant loss(PDL) in tilted fiber Bragg grating: Application of a PDL equalizer," IEEE Proc. Optoelectron. **149**(5), 211–216 (2002).

1. Introduction

Since the first fiber Bragg grating was invented by Hill in 1978 [1], and the invention of UV transverse inscription technology reported by Meltz in 1991 [2], optical fiber gratings have been extensively investigated and attracted much more interests in their applications. In the past 20 years, the fiber grating technologies have been developed to a range of grating types including fiber Bragg gratings (FBGs), long period fiber gratings (LPGs), modified fiber Bragg grating (including chirped (CFBG), sampled (SFBG) and Moiré structures (MFBGs)) and tilted fiber gratings (TFGs). The TFGs with an asymmetric grating structure have very strong polarization dependent mode coupling behavior between core mode and cladding/radiation modes, which depends on the parameters of grating including the tilt angle and period. According to the mode coupling mechanism, the TFGs can be simply sorted as tilted fiber Bragg gratings (TFBGs), 45° TFGs and excessively TFGs. The TFBGs have dense backward propagating cladding mode resonances in the transmission spectrum, which have been used to achieve fiber based surface plasma resonance (SPR) sensor [3], humidity sensor [4], accelerometer [5], water level sensor [6], twist sensor and so on. 45°-TFGs show very high polarization extinction ratio, functioning as ideal in-fiber linear polarizers [7,8], which have been used as polarimeter [9], optical fiber spectrometer [10] and power taping device [11]. The excessively TFGs were firstly reported by Zhou et al in 2006 [12]. Due to their unique polarization property, Ex-TFGs have been used as refractive index, twisting, transverse loading, and water level sensors [13,14, 16, 17]. Research about TFBGs from J. Albert's group has revealed the cladding modes coupled from a TFBG were split into two sets

of polarization dependence cladding modes (TE and TM mode) [3,18–20]. In addition to TFBGs, there were also several papers which have given theoretical modeling about the transmission spectra of tilted gratings with long period pattern [21,22]. Recently, Mou et al have published a review chapter about sensing applications using Ex-TFGs [23], and we have reported a high Q factor and sensitivity glucose sensor by using an Ex-TFG [24]. Although abundant experimental works on Ex-TFGs reported, there is no report giving a detailed theoretical and experimental analysis about the dual polarization dependent peaks of Ex-TFGs. In this paper, we report a detailed investigation of the dual-peak feature of Ex-TFGs in numerical analysis and experiments.

2. Numerical analysis of Ex-TFG

A transmission fiber consists of a small radius core with high refractive index and a large cladding layer of low refractive index. The mode effective index could be obtained by solving the Maxwell's equations. As an approximate calculation, the cladding mode index may also be calculated by treating the cladding as a coreless rod surrounded by air. However, the refractive index difference between cladding and air cannot be neglected in the calculation. In [25,26], the eigenvalue equations for TM_{0m} and TE_{0m} are given as Eq. (1) and Eq. (2), respectively.

$$\frac{J_1(u)}{uJ_0(u)} + (1-2\Delta n)\frac{K_1(w)}{wK_0(w)} = 0 \qquad (1)$$

$$\frac{J_1(u)}{uJ_0(u)} + \frac{K_1(w)}{wK_0(w)} = 0 \qquad (2)$$

where, Δn is the refractive index difference between the cladding and air; $u = 2\pi r(n_{cl}^2 - n_{cleff}^2)^{1/2}/\lambda$ and $w = 2\pi r(n_{cleff}^2 - n_{air}^2)^{1/2}/\lambda$ (r is the radius of fiber cladding; n_{cleff}, n_{cl}, and n_{air} are the mode index of cladding, the refractive index of cladding material and the refractive index of air, respectively).
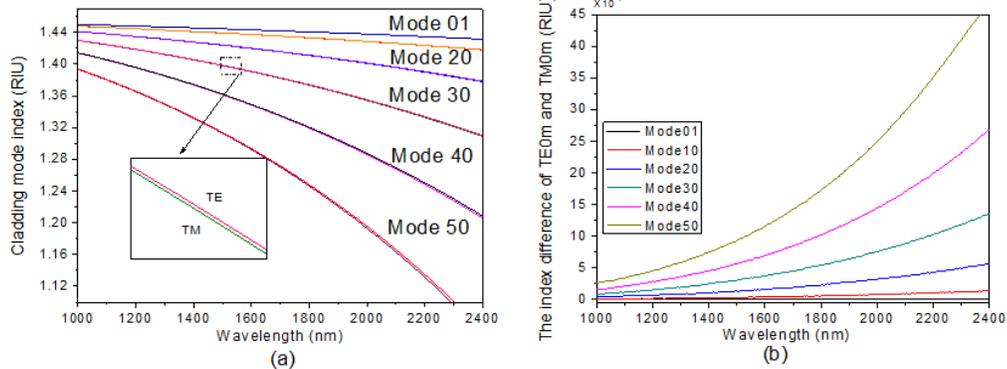

Fig. 1. (a) The mode indexes of TE and TM cladding modes (inset shows the enlarged scale for 30th modes) and (b) the mode index difference between TE and TM cladding modes as a function of the wavelength.

The effective indexes of TM_{0m} and TE_{0m} cladding mode could be obtained by solving the Eq. (1) and Eq. (2). Due to the significant index difference between the cladding and air, there is a slight difference between the effective indexes of TE_{0M} and TM_{0M} cladding modes. Figure 1(a) shows the calculated effective indexes of the TE and TM cladding modes for standard single mode telecom fiber (SM-28). The inset of Fig. 1(a) shows the effective indexes of 30th cladding mode in a small wavelength range, in which it can be clearly seen that the effective index of TE cladding mode is a bit larger than the TM one. Figure 1(b) shows the effective index differences for six TE and TM cladding modes of different orders (1st, 10th, 20th, 30th,

40th and 50th) as a function of wavelength. As it shown in the Fig., the index difference between TE and TM modes is increasing with increasing mode order and wavelength.
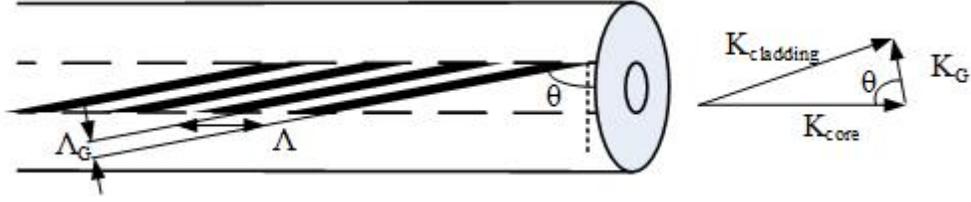

Fig. 2. The schematic and vector phase matching diagram of an Ex-TFG.

Phase match condition

Because of circular symmetric structure, the birefringence in a standard single mode fiber is almost negligible. The asymmetric UV-exposure during fiber grating inscription could induce birefringence in the optical fiber [27], but it is very small and could be ignored in normal case. However, the tilted index modulated plates inscribed inside of the fiber core have broken the circular symmetric, inducing significant birefringence to the fiber core. Thus, the TFGs could couple the orthogonal TE and TM core modes into TE and TM cladding modes, respectively.

The phase match condition is the most important parameter of a fiber grating, which determines the wavelength of the strongest coupling between the core and cladding modes. The phase match condition for an Ex-TFG is expressed as [28]:

$$\lambda = (n_{co}^{eff}(\lambda) - n_{cl,m}^{i,eff}(\lambda))\frac{\Lambda_G}{\cos\theta} \qquad i = \text{TE or TM} \qquad (3)$$

where λ is the resonance wavelength; n_{co}^{eff} is the effective index of the core mode at the wavelength λ; $n_{cl,m}^{i,eff}$ is the effective index of mth TE/TM cladding mode at the wavelength λ; Λ_G is the normal period of grating; θ is the tilt angle of the grating.

The relationship between the axial period (Λ), normal period (Λ_G) and the tilt angle (θ) of a TFG is shown in Fig. 2, which is expressed as:

$$\Lambda = \frac{\Lambda_G}{\cos\theta} \qquad (4)$$

Substituting Eq. (4) into Eq. (3), the phase matching condition for an Ex-TFG can be rewritten by using the axial period of grating as:

$$\lambda = (n_{co}^{eff}(\lambda) - n_{cl,m}^{i,eff}(\lambda))\Lambda \qquad i = \text{TE or TM} \qquad (5)$$

From Eq. (5), we notice that the response wavelength of Ex-TFG is determined by the mode indexes of core and cladding and the axial period of grating.
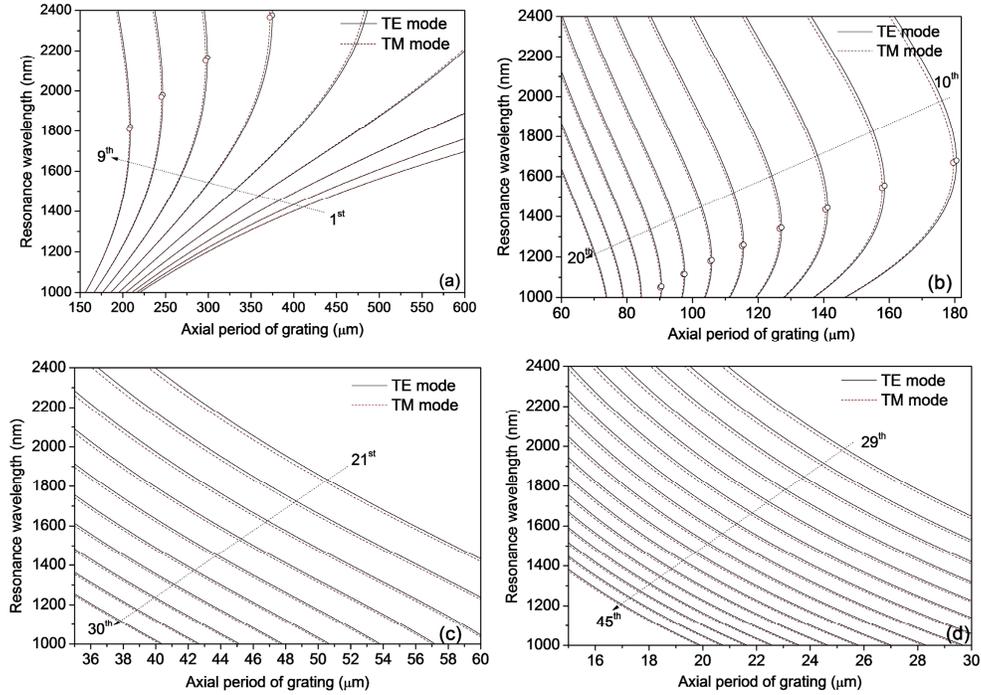
Fig. 3. Simulated resonance wavelength versus the axial period of Ex-TFG with TE (solid line) and TM (dash line) modes for different orders: (a) m = 1 to 9; (b) m = 10 to 20; (c) m = 21 to 30; (d) m = 29 to 45.

For an Ex-TFG, the tilted grating structure causes TE and TM polarization of fundamental core mode couple into forward propagating TE and TM cladding mode, respectively. This is the reason that the transmission spectrum of an Ex-TFG exhibits a series of polarization dependent dual peaks, as will be clearly shown in the experimental results below. By applying phase matching condition in Eq. (5), a set of phase matching curves are generated and plotted in Fig. 3 for 45 TE (solid line) and TM (dash line) cladding modes covering a broad wavelength range from 1μm to 2.4μm: with mode order m = 1 to 9, m = 10 to 20, m = 21 to 30 and m = 29 to 45 shown in Fig. 3(a)-3(d), respectively. As displayed in the figures, for each mode index, there are two curves corresponding to TE and TM coupling. Furthermore, there is a dispersion turning point ($d\lambda/d\Lambda = \infty$) for each mode, and the corresponding wavelength of dispersion turning point is moving to shorter wavelength with increasing mode order [29]. From Fig. 3, we also notice that the resonance wavelength of TM cladding mode is longer than that of the same order TE mode before reaching the turning point, and conversely the wavelength of TE mode is longer than the one of the same order TM mode after reaching the turning point.

Because of the coupling to such TE and TM dual cladding modes, transmission spectrum of an Ex-TFG will show two sets of polarization dependent peaks. By using the analysis method reported in [30], we can give a general expression of spectral response of the TM and TE modes of an Ex-TFG:

$$\Delta\lambda = \lambda_{TM} - \lambda_{TE} = \frac{\Delta n_{cl,m}^{(TE-TM),eff} \Lambda}{1 - \Lambda(\frac{dn_{co}^{eff}}{d\lambda} - \frac{dn_{cl}^{TM,eff}}{d\lambda})} = \gamma_{TM} \ \Delta n_{cl,m}^{(TE-TM),eff} \Lambda \qquad (6)$$

where, γ_{TM} is the γ factor of *TM* cladding mode; Δn is the cladding mode index difference between *TE* and *TM*. We set the λ_{TE} at 1300nm, 1550nm and 1700nm, and the dual peaks

separation as a function of mode order can be calculated and plotted in Fig. 4. The separation gap is very large at the mode around the turning point. Meanwhile, the resonance wavelength of TM mode is longer than the TE mode as $d\lambda/d\Lambda>0$, and shorter as $d\lambda/d\Lambda<0$. The Fig. 4 also shows that the longer resonance wavelength is, the larger separation between TE and TM modes.
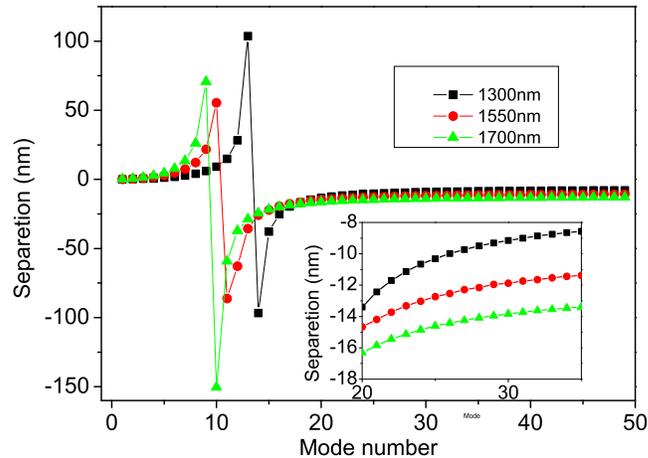

Fig. 4. The separation of TM and TE resonance cladding modes as a function of mode order for 1300nm, 1550nm and 1700nm. Inset in Fig. 4 shows the enlarged separation data from mode 20 to 35.

3. Fabrication of Ex-TFG

To achieve forward-mode coupling, an Ex-TFG must have an excessively tilted structure at an angle close or larger than 70° to overcome total internal reflection. However, due to its relatively smaller period (typically in tens μm) and the excessively tilted structure, such gratings cannot be fabricated by the point-by-point technique. A more realistic method would be using a tilted amplitude mask. In this work, we used a custom-designed amplitude mask with a period of 6.6μm. This period was designed to ensure that grating responses generated from high order cladding modes coupling will be centered in the C-L band.
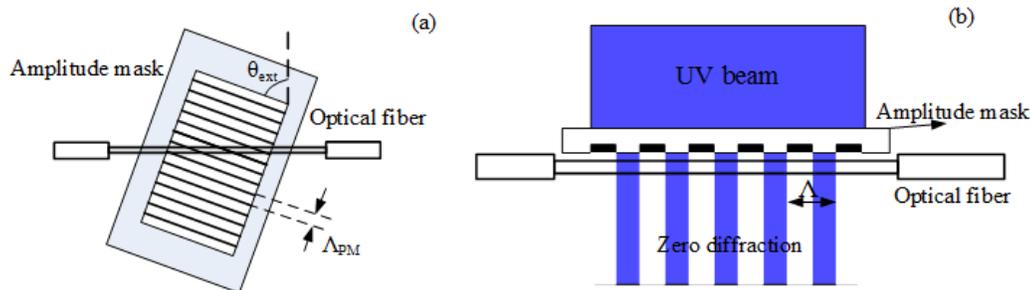

Fig. 5. Schematic of (a) the front view and (b) the top view of amplitude mask and fiber with 0 order diffraction inside the fiber core.

As it shown in Fig. 5(a) and 5(b), in the inscription, the fiber is placed in the front of tilted amplitude mask. Because it is an amplitude mask, the zero order diffraction of UV beam passed through the mask was used to inscribe grating into the fiber core, in which fiber grating and the amplitude mask have the same the axial period. The mask with 6.6μm normal period tilted at 76.5° would result in a 28.2μm axial period (the axial period could be

calculated from Eq. (4) and Eq. (6). Due to the cylindrical geometry of fiber, the tilt angle of UV fringe outside of fiber is different to that inside of fiber, which has been reported in [31]. According to the calculation, the amplitude mask tilted at ~76.5° would produce a highly tilted fringes at ~81° in the fiber core. The relationship between the grating period, the external tilted angle and period of amplitude mask can be expressed as:

$$\Lambda_G = \frac{\Lambda_{AM}\cos(\frac{\pi}{2}-\tan^{-1}\left[\frac{1}{n_{UV}\tan(\theta_{ext})}\right])}{\cos\theta_{ext}} \qquad (7)$$

where, Λ_G and Λ_{AM} are the grating period inside the fiber and the amplitude mask, respectively; n_{UV} is the refractive index of fiber (around 1.52) at the wavelength of 244nm; θ_{ext} is the tilt angle of mask.

4. Experimental results for Ex-TFGs

In the experiment, we have evaluated the transmission spectra of an 81°-TFG. Figure 6(a) depicts the transmission spectrum of the 81°-TFG from 1300 to 1700 nm, which was measured by an unpolarized broadband ASE light source. It can be seen clearly from the figure that all peaks split into two, generated from the coupling to the two sets of cladding modes of orthogonal polarization statuses, in which there are 7 pairs of dual peaks at the wavelength range between 1300nm and 1700nm. However, according the simulation results, only 5 pairs of dual peaks are existing between 1300nm and 1700nm. Three reasons might cause this discrepancy: (1) the simulation model used in this paper is a two layer waveguide structure, which is a simple and approximate model, and cannot present the real waveguide structure; (2) the average index modulation induced by UV-exposure wasn't considered in the calculation; (3) the fabrication process may cause inaccuracy in tilted angle (during the fabrication process, tilt angle of mask is controlled by a goniometer, however, it is difficult to accurately control the tilt angle, which might have a $\sim\pm1°$ deviation).
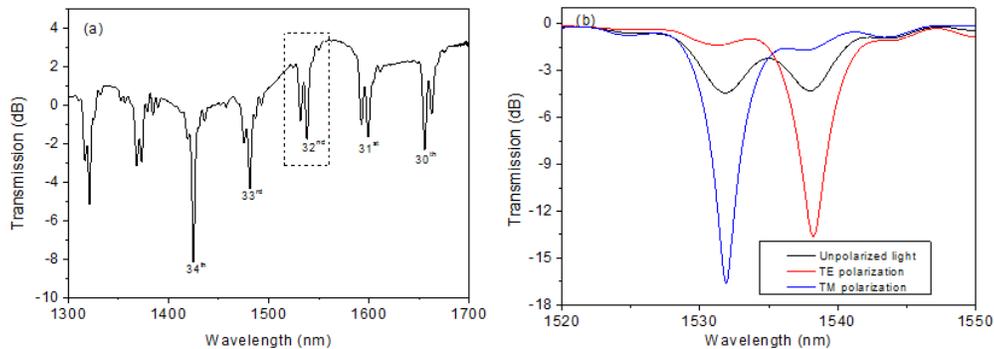

Fig. 6. The transmission spectra of 81°-TFG: (a) a series of dual-peak resonances from 1300 to 1700 nm and (b) zoomed dual peaks at around 1530nm when launched with unpolarized light (black line) and orthogonally polarized lights (blue line – TM and red line - TE).

The zoomed spectra of one pair of the dual-peak at around 1550nm when measured with unpolarized and polarized light are shown in Fig. 6(b). As shown clearly in the figure, when the grating launched with unpolarized light, the two peaks are coupled with almost the same strength showing ~3dB transmission loss, and when it launched with orthogonally polarized lights, one peak is fully excited and the other is almost diminished. According to previous calculation results, for SM-28 fiber, the resonance mode at around 1530nm should be the 32nd cladding mode, and the wavelength of TM mode should be shorter than that of the TE

mode, thus, we identify the 1532nm peak in Fig. 6(b) is the coupling to the TM mode and 1538.8nm peak is the TE mode.
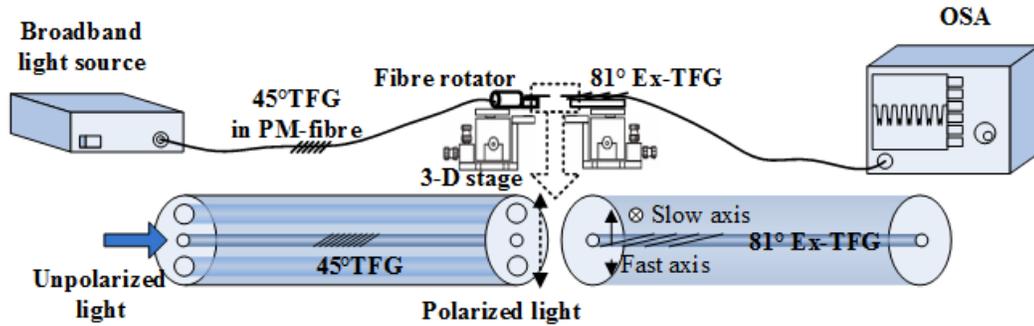

Fig. 7. The experimental setup investigating the polarization dependent loss of the 81°-TFG.

The polarization dependent loss of the 81°-TFG was further investigated using the setup shown in Fig. 7, in which there are a broadband light source, an in-fiber linear polarizer based on 45°-TFG in a PM fiber, a fiber rotator, two 3-D stages and an optical spectrum analyzer. The linearly polarized light from the 45°-TFG is butt-coupled to the 81°-TFG. The output spectrum of 81°-TFG is measured by the optical spectra analyzer. Using the setup shown in Fig. 7, the linearly polarized light with different orientations can be launched into the 81°-TFG. During the measurement, this was facilitated by simply rotating the PM fiber amounted on the fiber rotator from 0° to 90° at a 15° increment. The evolving transmission spectra were recorded and shown in Fig. 8(a). When the angle is at 0°, the linearly polarized light is at TM polarization, i.e. the polarization is aligned in the equivalent fast-axis of 81°-TFG, thus fully exciting the TM peak at the shorter wavelength side and eliminating the one at longer wavelength. When the input PM fiber is rotated by 45°, the two peaks are at the same strength of 3dB (50%). Finally, when the angle reaches 90°, the polarized light is TE polarization and the peak at the longer wavelength is fully excited and the peak at the shorter wavelength is totally disappeared.
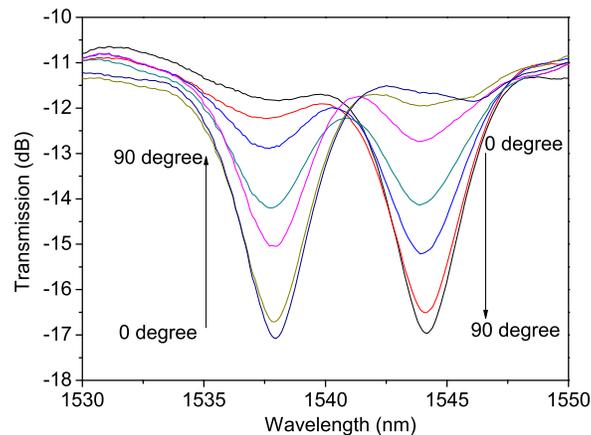

Fig. 8. the transmission spectra of 81°-TFG measured by launching a linear polarization light with different azimuth angles with respect to the fast axis of grating.

According to our theoretical analysis, the dual peak feature of Ex-TFG is caused by the different mode index of TE and TM cladding mode, which is because the eigenvalue equation of TM cladding mode is not only affected by the surrounding medium refractive index (SRI), but also by the index difference between cladding and surrounding medium (see in Eq. (1)

and (2)). Then the SRI is increasing, the mode indexes of TM and TE cladding mode are changing, and the index difference between TE and TM mode is decreasing.
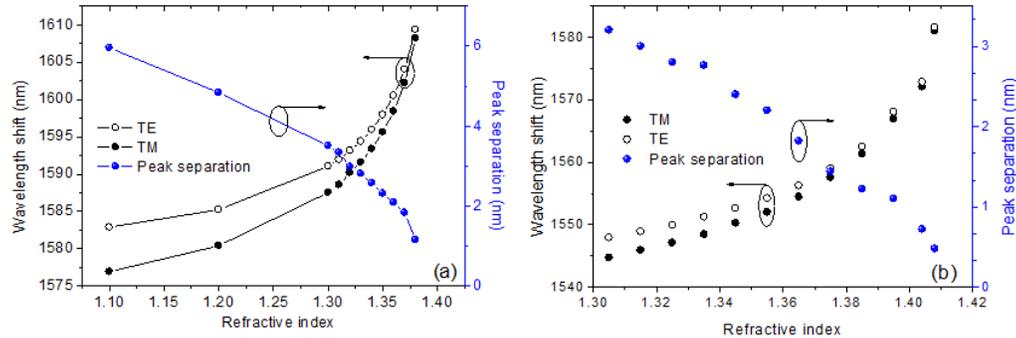

Fig. 9. The simulated (a) and experimental (b) results of peak separation of 32nd dual peak cladding mode versus surrounding medium refractive index.

As shown in [15], the dual peaks of Ex-TFG have emerged into one peak, when the SRI is at 1.35. However, in our experiment, there were still two peaks when the index gel of SRI = 1.35 was applied to the grating under the polarized light. We have investigated the TE and TM cladding mode versus the different SRIs, and examined the peak separation of 32nd dual peak in simulation and experiment. The results are depicted in Fig. 9, in which the simulated results showing the peak separation gap is around 6nm at SRI = 1, and the experimental result indicating it is around 6.8nm at SRI = 1. As increasing the SRI, the separation gap from simulated results is gradually decreasing to 1.2 nm at the SRI = 1.38 (See in Fig. 9(a)), and that from experimental results reached to 0.48nm at the SRI of 1.408 (See in Fig. 9(b)). With further increasing SRI, because the SRI is higher than the guided cladding mode index, the cladding then can no longer be supporting any cladding modes. Although the simulated results have not matched exactly with the experimental results, however, their variation trends agreed very well, and both have clearly shown the separation gap of dual-peak of Ex-TFG is decreasing as increasing of SRI.

5. Conclusions

We have theoretically and experimentally investigated the mode coupling property and spectral function of Ex-TFGs. Due to the fiber symmetry break induced by the excessively tilted structure, all cladding modes are degenerated into two sets of orthogonal polarizations (TE and TM), showing dual-peak feature on their spectral response. The polarization dependent loss varies according to the polarization status of the launched light, resulting in one set of polarization modes complete excited and the other eliminated. By launching linear polarized light, the Ex-TFGs are confirmed to have TM and TE cladding modes. We have also investigated the separation of dual peaks theoretically and experimentally and the results have revealed that the dual-peak gap is decreasing as the increase of SRI. All experimental outcomes are in good agreement with our theoretical analysis results.

Acknowledgments